MmWave Fronthaul-to-Backhaul Interference in 5G NR Networks

Edgar Jirousek*†, Zeyu Huang*†, Stefan Pratschner*†, Robert Langwieser†, Stefan Schwarz*† and Markus Rupp†
*Christian Doppler Laboratory for Dependable Wireless Connectivity for the Society in Motion
†Institute of Telecommunications, TU Wien, Austria, Email: edgar.jirousek@tuwien.ac.at

***Abstract*—Fixed point-to-point microwave links (P-P links) are widely used for vital backhaul connections in cellular networks. One frequency range allocated to P-P links by the International Telecommunications Union ranges from 24.25 GHz to 29.5 GHz. The same frequency range was also allocated to mobile services, with bands dedicated to 5G new radio (NR). Potential outages or performance drops in P-P links due to interference from 5G NR are therefore a concern to mobile network operators. We characterize the link-level performance of a commercial off-the-shelf (COTS) P-P link experimentally through measurements. We install a COTS P-P link on our campus. Through an additional experimental transmitter, we generate a 5G NR interference signal, allowing us to measure the link performance depending on signal-to-interference ratio (SIR) in the field. We measure the data rate that the P-P link achieves with respect to the interferer's location and transmit power. We establish a relation between the P-P link's SIR and data rate based on our measurements. We further measure the P-P link's antenna pattern in an anechoic chamber. To investigate the impact of interfering 5G NR user equipments (UEs) in typical cellular network deployment, we perform system-level simulations based on our link-level measurements. We simulate the impact of 5G NR users on a P-P links backhaul connection in typical cell geometries. We identify the cell's key parameter that determines the P-P link's achievable data rate.**

***Index Terms*—millimeter wave, 5G NR, fronthaul, backhaul**

I. Introduction

Fixed point-to-point microwave links (P-P links), also known as fixed links, or point-to-point radio, are often mounted on the same tower as a base station (BS) for cellular networks. P-P links serve as nodes for backhaul connections between the BS and the core network. P-P links need to function highly reliably to fulfill their vital role as backbone connections in cellular networks. Interference from other nearby services is detrimental to P-P links' operation. In this paper, we focus on P-P links that operate in the 24.25 GHz - 29.5 GHz range (26 GHz band). The International Telecommunications Union (ITU) allocates the 26 GHz band to fixed services, such as P-P links, and mobile services [1, pp. 158-160]. For mobile services, the 3rd Generation Partnership Project (3GPP) defined operating bands for 5G new radio (NR) that cover the entire 26 GHz band [2]. Hence, 5G NR user equipments (UEs) are potential causes of interference for P-P links in the 26 GHz band. There exists a lot of research that considers the deployment of directional links for fronthaul or backhaul in 5G and beyond, see [3]–[6] for example. Therefore, the interference problem is relevant for future cellular networks. Several methods to mitigate interference have been proposed [7]–[15], but these methods are not applicable to currently employed commercial off-the-shelf (COTS) P-P link hardware. Additionally, the European Conference of Postal and Telecommunications Administrations (CEPT) studied BS's and UE's interference to P-P links, and concluded protection distances between P-P links and 5G NR [6], though not based on measurements. We provide a measurement-based study on P-P link's susceptibility to interference from 5G NR UEs.

We install a COTS P-P link on our campus. We transmit Transmission Control Protocol (TCP) data over the P-P links in one direction. We build a custom interferer that radiates a 5G NR signal towards the receiving P-P link's terminal, at the same polarization and frequency. At the receiving P-P link terminal, we measure the TCP data rate. We experiment with different interferer transmit powers, to establish a relation between the signal-to-interference ratio (SIR) and data rate for the P-P link. We repeat the experiment by placing the interferer at two separate locations at our campus, to ensure repeatability of our measurements. In addition to the SIR - data rate relation, our simulations require the P-P link's antenna pattern. For our simulations, the antenna pattern is especially important, due to the high directivity of antennas typically used in P-P links. The P-P link's susceptibility to interference thus varies greatly depending on an interfering UE's location. Therefore, we measure the P-P link's antenna pattern in an anechoic chamber. The relation between SIR and data rate, and the antenna pattern serve as a basis for a model that we establish, in order to simulate a P-P link's performance when multiple 5G NR users are nearby. We use our results to derive transmit power thresholds for users in a P-P link's vicinity, such that certain coverage probabilities is still provided.

The impact of interference on the P-P link can be characterized by the coverage probability. The stochastic geometry based method is a crucial way to study the stochastics of the coverage probability [16], [17]. The coverage probability can be obtained in different ways. In [18], [19] different analytical expressions under different assumptions for the coverage probability are calculated. This kind of analytical approach usually needs several assumptions to make the calculation tractable.

In this paper, we use a Monte Carlo simulation to obtain

This work has been funded by the Christian Doppler Laboratory for Dependable Wireless Connectivity for the Society in Motion. The financial support by the Austrian Federal Ministry for Digital and Economic Affairs, the National Foundation for Research, Technology and Development and the Christian Doppler Research Association is gratefully acknowledged.

the P-P link's coverage probability for different amounts of interfering 5G users and their radiated power in the vicinity of the P-P links.

The paper is organized as follows: We describe our measurements and their results in Section II. Section III provides a typical interference scenario for a P-P link and the simulated results. Finally, we conclude our paper in Section IV.

Contribution: We experimentally characterize a COTS P-P link on a link-level. We (i) measure the P-P link's data rate as a function of SIR in the field and (ii) measure the P-P link's antenna pattern in an anechoic chamber. We use our measurement results as a basis for a system-level simulation, where we establish a relationship between the number of interfering users and the transmit power of each user for a given coverage probability. We provide a basis for guidelines for harmonizing 5G NR system deployments and P-P links in the 26 GHz band. We express the minimum data rate that a P-P link can provide a given probability in cells with different BS heights, radii, and users. We identify that key parameter of the cell that determines the P-P link's achievable data rate.

II. Link-Level Measurements

We conduct two measurements with a COTS P-P link:

(i) We study a COTS P-P link's susceptibility to interference from 5G NR in the field. We install and operate a P-P link at our campus. The P-P link consists of two nodes. Each node consists of two components, a radio unit (RU), and a modem unit (MU). The RU consists of a highly directive antenna, and converts the radio signal to an intermediate frequency for the MU and vice versa. The MU converts Ethernet data streams to an intermediate frequency for the RU, and vice versa. The MU further serves as a node for Internet Protocol traffic. We build a custom interferer that radiates a 5G NR signal. We point the interferer's antenna towards the P-P link RU that receives a data stream from another P-P link RU. We vary the interferer's transmit power, and record the P-P link's data rate each time. We perform the same measurement when placing the interferer at two locations on our campus. We thereby ensure that our measurements are reproducible.

(ii) We measure the P-P link's antenna pattern in an anechoic chamber. The P-P link's antenna is highly directional, thus its received interference power depends strongly on the interferer's location as well as the interferer's transmit power. We use the results for both measurements as a basis for our simulations in Section III.

Microwave Link

We install a pair of RUs (Ericsson MINI-Link) on two opposing roofs at our campus in Gusshausstrasse 25, Vienna, 159 meters (m) apart, as shown in Fig. 1. P-P link Tx denotes the node that transmits the TCP data signal. P-P link Rx receives the signal from P-P link Tx and the 5G NR interference signal. The P-P link uses frequency division duplex. We set the P-P link to use the center frequencies 25.319 GHz (lower band, Tx to Rx) and 26.327 GHz (upper band, Rx to Tx), a bandwidth of 28 MHz each, and vertical polarization. The

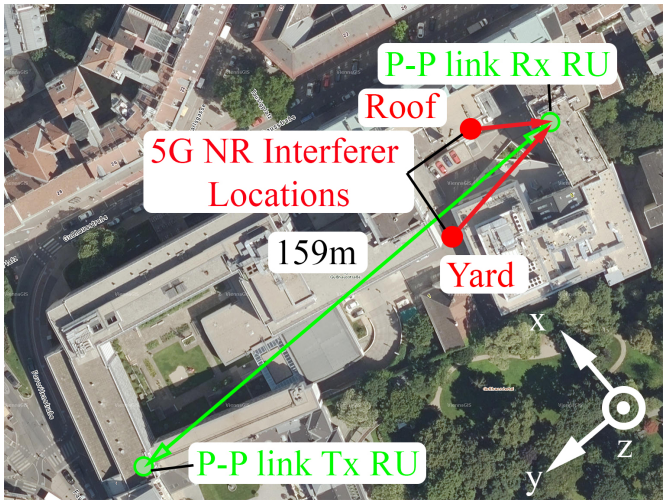

Fig. 1. Top view of the P-P link RUs on our campus and the two interferer locations [20].

P-P link RUs transmit at an average power of -10 dBm, and receive an average power of -40 dBm from each other. Each RU is connected to an MU.

Interferer

To artificially generate a 5G NR interference signal, we employ an experimental transmitter consisting of a signal generator, an amplifier, and a horn antenna. We generate an orthogonal frequency-division multiplexing (OFDM) signal in the P-P link's lower band with a Keysight M8195A Arbitrary Waveform Generator. The signal consists of 224 64-QAM modulated subcarriers, spaced 120 kHz apart, from 25.30560 GHz to 25.33236 GHz. We feed the signal to an RF-Lambda RFLUPA18G47GCK power amplifier. We feed the amplified signal to a Vector Telecom VT260SGAH25K2.92K horn antenna with 25.4 dBi of gain in co-polarization with the RU. We use a directive horn antenna to increase the maximum interference power at the P-P link Rx. This allows us to study the P-P link's behaviour in SIR ranges that are not described by the manufacturer. We measure the P-P link's data rate when placing the interferer at the two locations on our campus which are described in Tab. I, according to the coordinate axes in Fig. 1, where P-P link Rx RU lies in the origin.

Entity	x-coordinate	y-coordinate	z-coordinate
P-P link Rx RU	0 m	0 m	0 m
P-P link Tx RU	0 m	159.2 m	-3.7 m
Interferer Location Yard	0.5 m	42.2 m	-28.6 m
Interferer Location Roof	12.9 m	16.8 m	-2.9 m

TABLE I
Coordinates of the P-P link RUs and the interferer locations.

Interference Measurement in the Field

Fig. 2 shows a schematic of our measurement setup, and Fig. 3 shows a photo of our measurement. We connect each MU to a computer that runs iPerf3 [21]. We configure the

P-P link to emulate a layer 1 connection between the two iPerf hosts. We transmit TCP data with iPerf in one direction only, at the P-P link's lower band. We point our interferer's antenna at P-P link Rx. The iPerf data traffic is isolated from other networks. The receiving iPerf client measured and stored the payload data rate. During the data rate measurement, our

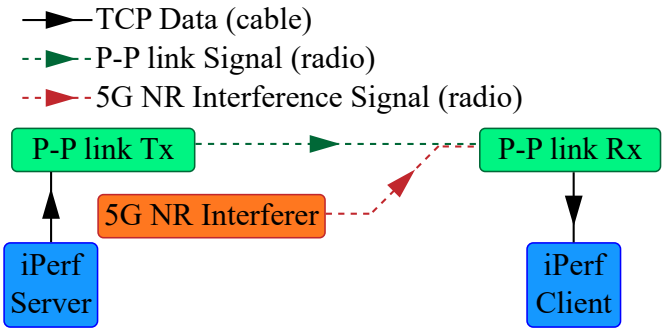

Fig. 2. Schematic of the interference measurement setup.

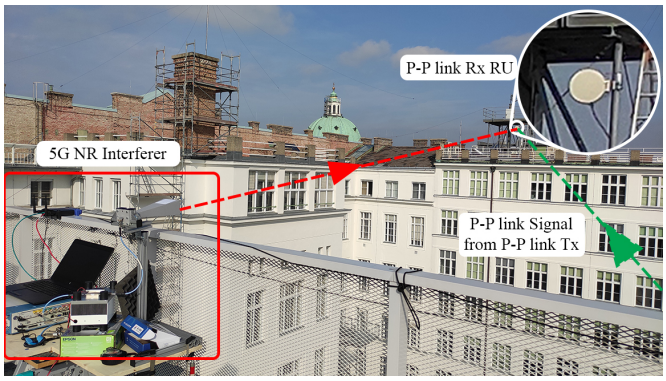

Fig. 3. Photo of the interference measurement setup.

interferer is turned on and transmits at 100 % duty cycle. We measure the SIR at the receiving RU as follows: We measure the received power from the transmitting RU P_{tr} when the interferer is turned off, and the received power from the interferer P_{ir} when the transmitting RU is turned off. We read P-P link Rx's received power from its command-line interface. We calculate the resulting SIR as

$$\mathrm{SIR}\big|_{\mathrm{dB}} = P_{\mathrm{tr}}\big|_{\mathrm{dBm}} - P_{\mathrm{ir}}\big|_{\mathrm{dBm}}. \quad (1)$$

We neglect the noise power, as it is 17 dB below our lowest recorded value of P_{ir} for 28 MHz bandwidth.

We configure the P-P link to employ adaptive modulation. We assume this to be the default setting for mobile network operators when employing a P-P link for backhaul connections. When using adaptive modulation, the P-P link adjusts the modulation order and resulting maximum data rate according to the SIR. Adaptive modulation ensures that a high SIR enables large data rates, while connection stability is still maintained for low SIRs. We set the highest modulation order to 512-QAM, and the lowest to 4-QAM. We omit data rate measurement results for the first 10 seconds (s) and stored results for the following 50 s.

Fig. 4 shows the measured average payload data rate for a 50 s interval with respect to SIR when placing the interferer at either of the two locations in Tab. I. The P-P link achieves its highest data rate of 173 megabits per second (Mbit/s) at SIR levels above 39 dB. Below 11 dB of SIR, the data rate drops to zero. The P-P link measures the received power in steps of 1 dB. The 1 dB quantization steps are shown as horizontal bars. Fig. 4 further shows how the P-P link adapts its modulation scheme to the SIR. The data rate increases in discrete steps with increasing SIR. Each step corresponds to one modulation scheme. The step corresponding to 4-QAM spans an SIR range of 10 dB. The remaining steps span 3-4 dB of SIR. The reason for the greater SIR span of the 4-QAM scheme is twofold: Firstly, the P-P link skips a possible 8-QAM, thus increasing the number of symbols by a factor of 4, rather than 2 for the remaining steps. Secondly, the 4-QAM interval ends abruptly with no reliable transmission below the 4-QAM step. We hypothesize that the P-P link prioritizes a decrease in modulation order over more error corrections when the SIR is low. We use the results from Fig. 4 to establish the relation

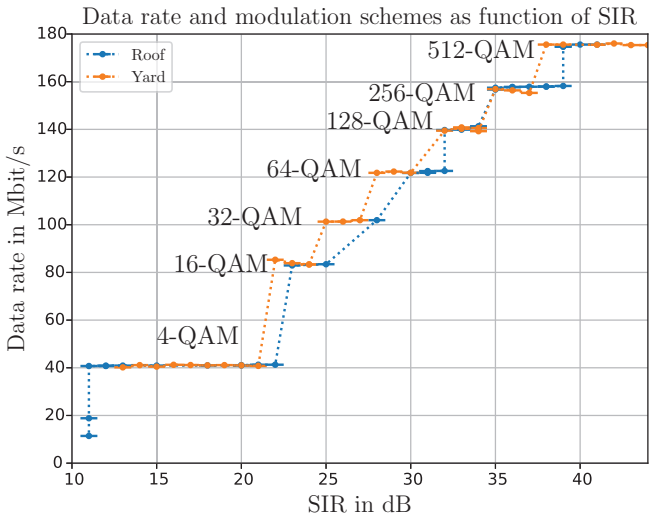

Fig. 4. Data rate and modulation scheme as function of SIR for adaptive modulation for the two interferer locations in Tab. I.

between SIR and data rate according to Tab. II.

SIR Range			Data Rate	Modulation Scheme
	SIR	$<$ 10.5 dB	0 Mbit/s	
10.5 dB $\leq$	SIR	$<$ 21.5 dB	41 Mbit/s	4-QAM
21.5 dB $\leq$	SIR	$<$ 24.5 dB	84 Mbit/s	16-QAM
24.5 dB $\leq$	SIR	$<$ 27.5 dB	101 Mbit/s	32-QAM
27.5 dB $\leq$	SIR	$<$ 30.5 dB	123 Mbit/s	64-QAM
30.5 dB $\leq$	SIR	$<$ 34.5 dB	141 Mbit/s	128-QAM
34.5 dB $\leq$	SIR	$<$ 37.5 dB	158 Mbit/s	256-QAM
37.5 dB $\leq$	SIR		175 Mbit/s	512-QAM

TABLE II
RELATION BETWEEN SIR AND DATA RATE FOR ADAPTIVE MODULATION.

Antenna Pattern Measurement

P-P links typically use highly directive antennas. Their gain is strongly angle-dependant. We take the gain's angle dependence into account in our simulations, in order to accurately model the resulting interference power from users at various locations. For this purpose, we measure the RU's antenna pattern in an anechoic chamber for 25.319 GHz. The measurement setup and the definitions of the angles ϑ and φ are shown in Fig. 5. The z-axis points in the direction of the P-P link's main lobe.

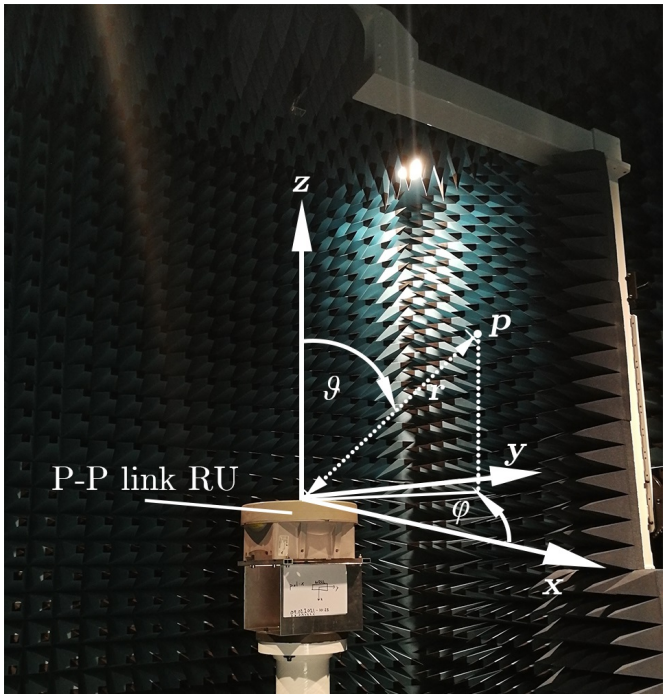

Fig. 5. P-P link RU antenna pattern measurement setup and definitions of the angles ϑ and φ in the antenna pattern for an arbitrary point p.

Fig. 6 shows the RU's antenna gain $G(\vartheta, \varphi)$ as a function of ϑ for $\varphi = 0°$ and $\varphi = 90°$ in co-polarization. At the main lobe, i.e., $\vartheta = 0°$, we measure a gain of 37.2 dBi. The antenna has a two-sided 6 dB beamwidth of 4° around the main-lobe, a first null beamwidth of 6°, and a side-lobe ratio of 23 dB.

III. System-Level Simulations

Based on our measurement results, we study the impact of interference from 5G NR UE on a P-P link in typical cells in this section. In this paper, we consider interference from nearby users around the receiving P-P link's RU.

Simulation scenario configuration

Fig. 7 shows the interference scenario that is considered in our simulation. The P-P link's RU is mounted on a BS tower. Interfering 5G NR UEs are scattered around the P-P link. Our simulation allows for an arbitrary amount of users around the P-P link. All the interfering users are on the ground below the P-P link. The users are distributed spatially uniformly on a disc. The P-P link's direct path is parallel to the disc. We

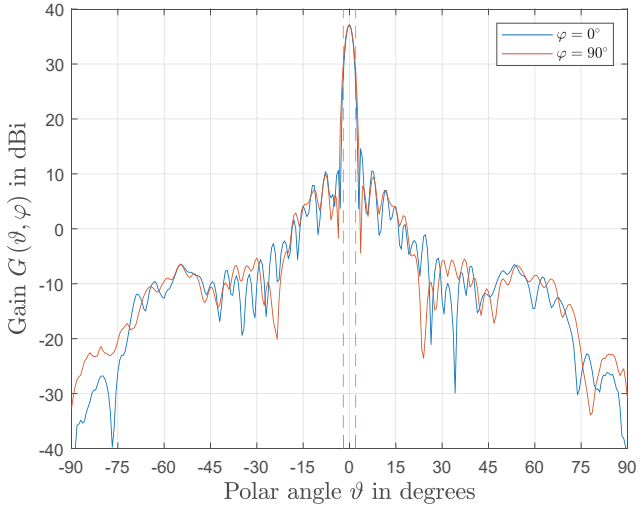

Fig. 6. P-P link antenna pattern for co-polarization at 25.319 GHz. At the red lines, the gain is 6 dB lower than at $\vartheta = 0°$.

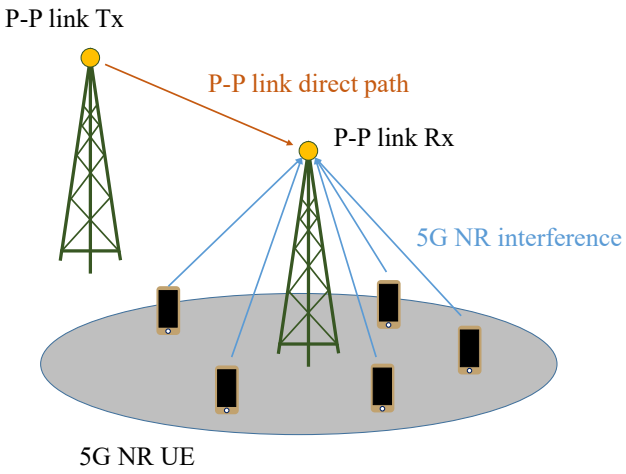

Fig. 7. Schematic of the simulated interference scenarios.

simulate different heights at which the P-P link is located above the disc. In our scenario, the interference power comes from all the scheduled users. For simplicity, the scheduled users are treated as to be in the P-P link's RU's far-field, while the far-field distance is calculated to be 15 m. We assume the mean transmit powers for all interfering users are the same, and they transmit at 100 % duty cycle. We model all the antennas of the scheduled users as isotropic. The users use the same frequency range and polarization as the P-P link. We assume a line of sight (LOS) path between each user and the P-P link's RU. Hence, the total interference power I from N scheduled users is

$$I = \sum_{i=1}^{N} P_{\mathrm{t}} G(\vartheta_i, \varphi_i) \left(\frac{\lambda}{4\pi r_i} \right)^2, \tag{2}$$

where P_{t} is the transmitted average power per user. The antenna gain is denoted with $G(\vartheta_i, \varphi_i)$. The angles ϑ_i and φ_i are defined as in Fig. 5, where the i-th user is located at

the point p. Thus, the z-axis is the direction of the P-P link's direct path. The distance between the i-th user and the RU is denoted with r_i, and λ is the free space wavelength of the employed center frequency.

We define the P-P link's coverage probability $P_c\left(P_\mathrm{t}, N, D_0\right)$ as the probability that the P-P link achieves a data rate D of D_0 or greater, when N users transmit at a mean power of P_t, i.e.

$$P_c\left(P_\mathrm{t}, N, D_0\right) \triangleq P\left[D \geq D_0\right]. \tag{3}$$

We limit D_0 to a data rate from Tab. II. We perform a one-to-one mapping from each data rate D_0 to the corresponding SIR interval's lower bound T_D in Tab. II. By further knowing that D increases monotonically with the SIR, we obtain the probability P_c that a data rate of D_0 can be provided as

$$P_c\left(P_\mathrm{t}, N, D_0\right) = P\left[\mathrm{SIR} \geq T_D\left(D_0\right)\right], \tag{4}$$

similar as in [18]. We assume that the received signal power at the P-P link is -40 dBm throughout our simulations.

We use the Monte Carlo method to obtain the coverage probability for each value of D_0. We simulate three scenarios in which a cell has the parameters in Tab. III. We define ϑ_min for each scenario as the smallest polar angle a user in the cell can come close to the P-P link's main lobe. We calculate the SIR values for each instantiation based on (2), and show which data rates can be provided with a coverage probability of 99.99 %.

Scenario	Height of P-P link above Disc	Disc Radius	ϑ_min
Scenario 1	2 m	100 m	1.5°
Scenario 2	15 m	100 m	8.5°
Scenario 3	15 m	1000 m	0.9°

TABLE III
CELL PROPERTIES FOR EACH SIMULATION SCENARIO.

Simulation Results

The P-P link is a backbone link between BSs. Hence the coverage probability is rigorous. Fig. 8 shows our results for cell 1. The regions between the lines in Fig. 8 show the data rate that can be provided with $P_c \geq 99.99\,\%$ for N users with average transmit power P_t. Each of the eight areas corresponds to one SIR interval in Tab. II. The data rate's monotonic decrease with respect to P_t causes each region to correspond to a larger data rate than the one above. The vertical displacements of the seven bordering lines correspond to the spans of each SIR interval from Tab. II. Again, we notice a 10 dB SIR span for a data rate of 41 Mbit/s, and 3-4 dB for the remaining data rates, except 175 Mbit/s and 0 Mbit/s, whose SIR intervals are half-bounded.

Fig. 9 shows our results for cell 2. The P-P link achieves greater data rates for the same value of P_t than in scenario 1. The P-P link is thus more robust to interference when located higher above users. In particular, 10 users have to transmit at $P_\mathrm{t} = 17$ dBm to cause a link outage in cell 1, 23 dB less than in scenario 2. Though this effect is in part due to the greater free space path loss, it is mainly due to the P-P link's antenna pattern. As the P-P link's height above the users increases, so does the polar angle ϑ_i for each user. Thus, each user will move further away from the P-P link's sharp main lobe, and consequently, cause less interference. In particular, ϑ_min is 1.5° for the cell 1 case, but 8.5° in scenario 2. While $\vartheta_\mathrm{min} = 1.5°$ still lies within in the P-P link's 6 dB beamwidth, $\vartheta_\mathrm{min} = 8.5°$ corresponds to a 29 dB gain reduction compared to $\vartheta_\mathrm{min} = 0°$.

Fig. 10 shows the results for scenario 3. The thresholds for P_t are 3-6 dB lower compared to scenario 2. This is due to the fact that $\vartheta_\mathrm{min} = 0.9°$ in scenario 3. Hence, interfering users can be closer to the P-P link antenna's main lobe. The larger antenna gain near the main lobe more than compensates for the average 20 dB greater free space path loss.

We show that the antenna pattern has a significant impact on the resulting data rate for a given coverage probability. We discuss the impact of ϑ_min and the scenario radius on the guaranteed data rate. We show that ϑ_min has the most decisive impact on a P-P link's data rate.

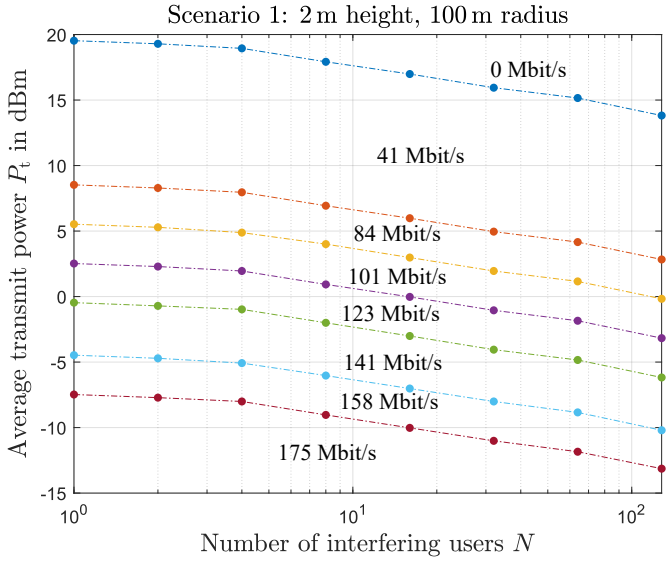

Fig. 8. Threshold transmit powers per user as function of the number of interfering users when the coverage probability is 99.99 % in scenario 1.

IV. CONCLUSION

P-P links play a vital role as backbones in cellular networks. They can experience notable performance drops when 5G NR users are nearby and operate at the same frequency. We conduct a measurement based link-level study on a COTS P-P link. We measure the impact of 5G NR interference on a P-P link in the field. We show the measured relation between SIR and data rate for a P-P link. We further measure the P-P link's antenna pattern. We use our link-level measurement results to conduct system-level simulations. We show a P-P link's guaranteed data rate in a cell for three typical geometries. We show that the most decisive impact on the P-P link's performance is determined by how close 5G NR users can approach the P-P link's antenna's main lobe, if the

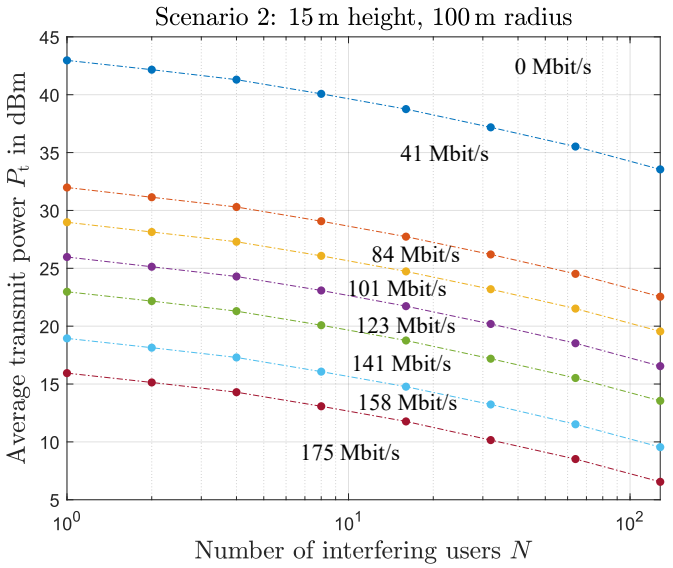

Fig. 9. Threshold transmit powers per user as function of the number of interfering users when the coverage probability is 99.99 % in scenario 2.

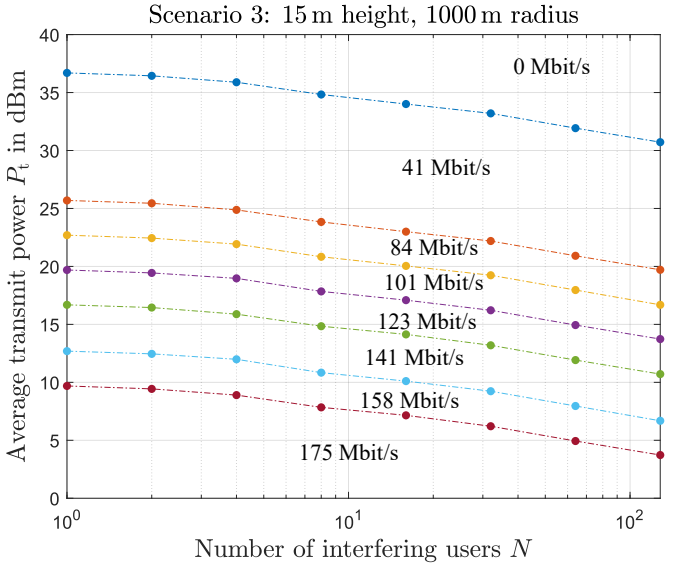

Fig. 10. Threshold transmit powers per user as function of the number of interfering users when the coverage probability is 99.99 % in scenario 3.

P-P link's RUs do not have significant side-lobes. Despite the P-P link's high antenna gain, 5G NR users can approach the main lobe and cause problematic interference to backhaul P-P links in a typical cell geometry.

References

[1] International Telecommunications Union (ITU), "Radio Regulations; Articles; Edition of 2020," 2020. [Online]. Available: http://handle.itu.int/11.1002/pub/814b0c44-en

[2] 3rd Generation Partnership Project (3GPP), "Technical Specification Group Radio Access Network; NR; Base Station (BS) radio transmission and reception (Release 17)," 3rd Generation Partnership Project (3GPP), TS 38.104, Jan. 2021.

[3] European Conference of Postal and Telecommunications Administrations (CEPT) Electronic Communications Committee (ECC), "Toolbox for the most appropriate synchronisation regulatory framework including coexistence of MFCN in 24.25-27.5 GHz in unsynchronised and semi-synchronised mode," CEPT ECC Report 307, Mar. 2020.

[4] Ping-Heng Kuo and A. Mourad, "Millimeter wave for 5G mobile fronthaul and backhaul," in *European Conf. Networks and Communications (EuCNC)*, 2017, pp. 1–5.

[5] S. Schwarz and S. Pratschner, "Dynamic distributed antenna systems with wireless mmwave fronthaul," in *53rd Asilomar Conference on Signals, Systems, and Computers*, 2019, pp. 569–575.

[6] European Conference of Postal and Telecommunications Administrations (CEPT) Electronic Communications Committee (ECC), "Guidance to administrations for coexistence between 5G and fixed links in the 26 GHz band," CEPT ECC Report 303, Jul. 2019.

[7] Z. Shi, Y. Wang, L. Huang, and T. Wang, "Dynamic resource allocation in mmWave unified access and backhaul network," in *IEEE 26th Annu. Int. Symp. Personal, Indoor, and Mobile Radio Communications (PIMRC)*, 2015, pp. 2260–2264.

[8] Y. Li, E. Pateromichelakis, N. Vucic, J. Luo, W. Xu, and G. Caire, "Radio resource management considerations for 5G millimeter wave backhaul and access networks," *IEEE Commun. Mag.*, vol. 55, no. 6, pp. 86–92, 2017.

[9] R. Taori and A. Sridharan, "Point-to-multipoint in-band mmwave backhaul for 5G networks," *IEEE Commun. Mag.*, vol. 53, no. 1, pp. 195–201, 2015.

[10] S. Rajagopal, R. Taori, and S. Abu-Surra, "Self-interference mitigation for in-band mmwave wireless backhaul," in *11th Consumer Communications and Networking Conf. (CCNC)*, 2014, pp. 551–556.

[11] A. Fouda, A. S. Ibrahim, I. Guvenc, and M. Ghosh, "Uav-based in-band integrated access and backhaul for 5G communications," in *Proc. IEEE 88th Vehicular Technology Conf. (VTC-Fall)*, 2018, pp. 1–5.

[12] M. N. Islam, N. Abedini, G. Hampel, S. Subramanian, and J. Li, "Investigation of performance in integrated access and backhaul networks," in *IEEE Int. Conf. Computer Communications Workshops (INFOCOM WKSHPS)*, Honolulu, HI, 2018, pp. 597–602.

[13] T. K. Vu, M. Bennis, S. Samarakoon, M. Debbah, and M. Latva-aho, "Joint in-band backhauling and interference mitigation in 5G heterogeneous networks," in *European Wireless 2016; 22th European Wireless Conf.*, 2016, pp. 1–6.

[14] R. Taori and A. Sridharan, "In-band, point to multi-point, mm-wave backhaul for 5G networks," in *IEEE Int. Conf. Communications Workshops (ICC)*, Sydney, Australia, 2014, pp. 96–101.

[15] M. Hashemi, M. Coldrey, M. Johansson, and S. Petersson, "Integrated access and backhaul in fixed wireless access systems," in *IEEE 86th Vehicular Technology Conf. (VTC-Fall)*, sep 2017, pp. 1–5.

[16] H. ElSawy, A. Sultan-Salem, M. Alouini, and M. Z. Win, "Modeling and analysis of cellular networks using stochastic geometry: A tutorial," *IEEE Commun. Surveys Tuts.*, vol. 19, no. 1, pp. 167–203, 2017.

[17] H. ElSawy, E. Hossain, and M. Haenggi, "Stochastic geometry for modeling, analysis, and design of multi-tier and cognitive cellular wireless networks: A survey," *IEEE Commun. Surveys Tuts.*, vol. 15, no. 3, pp. 996–1019, 2013.

[18] J. G. Andrews, F. Baccelli, and R. K. Ganti, "A tractable approach to coverage and rate in cellular networks," *IEEE Trans. Commun.*, vol. 59, no. 11, pp. 3122–3134, 2011.

[19] M. Z. Win, P. C. Pinto, and L. A. Shepp, "A mathematical theory of network interference and its applications," *Proceedings of the IEEE*, vol. 97, no. 2, pp. 205–230, 2009.

[20] Stadt Wien - ViennaGIS. Date last accessed: 04 March 2021. [Online]. Available: www.wien.gv.at/viennagis/

[21] iPerf – the TCP, UDP and SCTP Network Bandwidth Measurement Tool. (Date last accessed: March 01, 2021). [Online]: https://iperf.fr.